**PSFC/JA-08-22**

# Diagnosing ablator $\rho R$ and $\rho R$ modulations in capsule implosions using charged-particle spectrometry at the National Ignition Facility (NIF)

J.A. Frenje, C.K. Li, J.R. Rygg[a)], F.H. Séguin,
D.T. Casey and R.D. Petrasso[b),]
J. Delettrez[1], V.Yu. Glebov[1], T.C. Sangster[1],
O. Landen[2] and S. Hatchett[2]

18 June 2008

Plasma Science and Fusion Center,
Massachusetts Institute of Technology, Cambridge, MA 02139 USA

[1]Laboratory for Laser Energetics, University of Rochester, Rochester, New York 14623
[2]Lawrence Livermore National Laboratory, Livermore, California, 94550

[a)] Present address: Lawrence Livermore National Laboratory, Livermore, California, 94550.
[b)] Also Visiting Senior Scientist at the Laboratory for Laser Energetics, University of Rochester.

The work described here was supported in part by US DOE (Grant No. DE-FG03-03SF22691), LLE (No.412160-001G), LLNL (No.B504974), and GA under DOE (DE-AC52-06NA27279).

Submitted to *Physics of Plasmas.*

# Diagnosing ablator $\rho R$ and $\rho R$ modulations in capsule implosions using charged-particle spectrometry at the National Ignition Facility (NIF)

**J.A. Frenje, C.K. Li, J.R. Rygg[a)], F.H. Séguin, D.T. Casey and R.D. Petrasso[b)]**

*Plasma Science and Fusion Center, Massachusetts Institute of Technology, Cambridge, Massachusetts, 02139*

**J. Delettrez, V.Yu. Glebov and T.C. Sangster**

*Laboratory for Laser Energetics, University of Rochester, Rochester, New York, 14623*

**O. Landen and S. Hatchett**

*Lawrence Livermore National Laboratory, Livermore, California, 94550*

## Abstract

By fielding several, compact proton spectrometers at various locations around an ignition-capsule implosion at the National Ignition facility (NIF) [G.H. Miller, E.I. Moses and C.R. Wuest, Nucl. Fusion **44**, S228 (2004)], $\rho R$ and $\rho R$ modulations of the ablator for a failed implosion can be obtained through absolute measurements of knock-on proton (KO-P) spectra. For ignition capsules with a Cu-doped beryllium (Be) ablator, 50:50 mixture of deuterium-tritium (DT) fuel and ~1% residual hydrogen (H) by atom, failed implosions can be diagnosed for neutron yields ranging from ~$10^{11}$ to ~$5\times10^{16}$ and local $\rho R$s up to ~240 mg/cm$^2$. For capsules with an ablator of Ge-doped CH, which contains large amounts of H, failed implosions can be diagnosed for neutron yields ranging from ~$10^{10}$ to ~$3\times10^{16}$ and local $\rho R$s up to ~200 mg/cm$^2$. Prior to the first ignition experiments, capsules with a Cu-doped Be ablator (or Ge-doped CH ablator), more deuterium-lean fuel mixture and H-dopant levels up to 25% in the fuel will be imploded to primarily reduce the neutron yield. The HDT-filled Be capsule implosion, which can be diagnosed for neutron yields ranging from ~$5\times10^{9}$ to ~$5\times10^{16}$ and local $\rho R$s up to ~240 mg/cm$^2$, is more suitable to diagnose using KO-P's as the signal-to-background ratio is significantly higher than for an ignition-capsule implosion. In

addition, analysis of CH-ablator data obtained from analogous OMEGA [T. R. Boehly. D. L. Brown, R. S. Craxton *et al.,* Opt. Commun. **133**, 495 (1997)] experiments indicate that the shape of the KO-P spectrum is affected mainly by the ablator $\rho R$. Other effects such as ablator-density-profile variations, time evolution of the ablator $\rho R$, fuel-ablator mix and electron temperature variations typically predicted for the ablator play minor roles.

[a] Present address: Lawrence Livermore National Laboratory, Livermore, CA, 94550.
[b] Also Visiting Senior Scientist at Laboratory for Laser Energetics at Univ. of Rochester.

## I. Introduction

Ignition of an indirectly laser-driven capsule implosion at the National Ignition Facility (NIF) [1] requires careful tuning of the drive conditions to the capsule parameters [2-5]. Inadequate knowledge about the drive physics is therefore a serious concern, since an under-driven or over-driven capsule will leave too much or too little ablator mass as payload and thus reduce the performance of an implosion to the point it fails to ignite [2]. If the initial ablator is too thin, it burns through too quickly and the implosion fails to ignite due to preheat or instability issues, or if the initial ablator is too thick, the implosion velocity is too low and the implosion fails to ignite due to poor compression. To address this issue, we propose to accurately diagnose the areal density ($\rho R$) of the ablator using charged-particle spectrometry. By fielding several compact charged-particle spectrometers (spectrometer housing is less than 5 cm in diameter) [6] at various locations around a NIF implosion, $\rho R$ and $\rho R$ modulations of the ablator can be obtained through measurements of spectra of knock-on protons (KO-P) elastically scattered by primary DT neutrons [7]. The KO-P's have a well known birth spectrum ranging from 0 to 14 MeV, and as they traverse through the ablator they lose energy in proportion to the amount of material they pass through ($\rho R$). A $\rho R$ value for the portion of the implosion facing a given spectrometer can therefore be determined from the energy downshift and shape of the measured KO-P spectrum by applying a newly developed analysis technique, which utilizes Monte Carlo modeling [8] of an implosion and the plasma-stopping power formalism described in reference [9]. Using this technique, it is shown in

this work that the shape of the spectrum of the escaping KO-P can be used to diagnose a variety of ablator compositions for neutron yields up to ~$5\times10^{16}$ and ablator $\rho R$s up to ~240 mg/cm$^2$.

The work described herein improves and extends significantly the work by Nakaishi *et al*. [10], Li *et al*. [11] and Frenje *et al*. [12], who used a simple implosion model to relate the $\rho R$ to the KO-P yield. The work by Li *et al*. and Frenje *et al*. also brought considerable improvement on that of Nakaishi *et al*., who obtained a coarse KO-P spectrum in a single direction for a thin-glass micro-balloon capsule implosion, as their work involved simultaneous high-resolution measurements in several different directions of the KO-P spectrum produced in ICF-relevant capsule implosions. However, as noted by Frenje *et al.*, this yield method is subject to significant spatial-yield variations caused by magnetic fields surrounding an implosion prohibiting $\rho R$ modulations to be diagnosed. As a result, an average $\rho R$ can only be obtained from several spectrometers fielded around an implosion using this method. Very relevant to this work is that Seguin *et al.* [13] and Hicks *et al.* [14] demonstrated that the energies of the KO-P's are not affected when bang time occurs after the laser pulse (when the electrical field has decayed away). Measurement of the KO-P spectrum is therefore a much more powerful method than the yield method for diagnosing the ablator $\rho R$ of an implosion.

In addition, the KO-P measurements and analysis technique described herein will nicely complement and extend the work by D.C. Wilson *et al*. [15], D.G. Hicks *et al*. [16] and R.E. Olson *et al*. [17-18] that were carried out mainly at the OMEGA laser facility. Wilson *et al*. applied a technique, extensively used at OMEGA for the last decades [6,13,19], to determine the $\rho R$ of the ablator from the energy downshift of 14.7-MeV protons produced in surrogate D$^3$He gas-filled CH-capsule implosions; Hicks *et al*. implemented an x-ray radiography technique that measures time-resolved $\rho R$, mass and velocity of the ablator; and Olson *et al*. studied X-ray ablation rates in planar geometries for Cu-doped Be, high density carbon, and Ge-doped CH, among other materials. All these techniques have distinctly different but complementary strengths.

This paper is structured as follows: Section II and III describe the methods for diagnosing the ablator $\rho R$ in several types of NIF-capsule implosions, while Section IV describes the proposed ablator $\rho R$ measurements at the NIF. Section V discusses KO-P

measurements performed at OMEGA, similar in spirit to those proposed herein for the NIF. Section VI summarizes the main results.

## II. Diagnosing the ablator $\rho R$ of ignition-capsule implosions

The current design of the 285 eV indirect-drive ignition capsule consists of a cryogenic deuterium-tritium (DT) layer of 75 μm with the outer surface positioned at a radius of 1000 μm. The capsule, which is filled with DT gas in equilibrium at 0.3 mg/cm$^3$, has an outer ablator layer with thickness varying from 90 to 170 μm depending on the ablator composition. At least three ablator designs are under consideration [3-4, 20-24]. The first design is made of beryllium (Be), doped gradually with copper; the second design is made of CH, doped gradually with germanium; the third design, which is not discussed in this paper, is made of high density carbon.

Diagnosing the Be-ablator design can be done by utilizing the ~1% residual H (by atom) in the DT fuel, and measure the energy spectrum of the KO-P's produced in the fuel. As the KO-P's produced in the fuel at the fuel-Be-ablator interface lose the least amount of energy, the high-energy endpoint of the KO-P spectrum provides accurate information about the $\rho R$ of the remaining Be ablator. To quantitatively study how the Be ablator affects the KO-P spectrum, a Monte-Carlo code [8] was used to simulate burn-averaged KO-P spectra for two capsule implosions, which are similar to the failed one described in ref. [25]. The density and temperature profiles of the fuel and Be ablator used in the simulations are illustrated in Fig. 1a. As shown by Fig. 1a, the density and temperature profiles for the fuel were kept the same, while the density profile for the Be ablator was changed artificially to illustrate the effect of a varying $\rho R$ on the KO-P high-energy end point. In the simulations, the ablator profile extends out to a radius of 150 μm (top figure) and to a radius of 220 μm (bottom figure) corresponding to an ablator $\rho R$ of 105 mg/cm$^2$ and 210 mg/cm$^2$, respectively. The resulting simulated KO-P spectra, shown in Fig. 1b, indicate high-energy endpoints at 10.0 MeV and 6.0 MeV, and thus energy downshifts of 4.0 MeV and 8 MeV for the 105 mg/cm$^2$ and 210 mg/cm$^2$ ablator, respectively. From these numbers it is evident that the energy downshift depends strongly on $\rho R$ and can be used to accurately infer the $\rho R$ of the remaining Be ablator [26]. This strong relationship is also illustrated in detail by the filled circles Fig. 2, which are the

results from several simulations. As shown by these data points, the Be ablator can be diagnosed for $\rho R$s up to ~240 mg/cm$^2$.

Electron temperature ($T_e$) variations typically predicted in the ablator do not significantly affect the $\rho R$ inferred from the energy downshift of the KO-P's. To change the inferred ablator $\rho R$ value by only 1%, one has to change $T_e$ in the analysis from ~100 eV to an unreasonable value of ~1000 eV. Measuring the high-energy end point of the KO-P spectrum is therefore a sensitive and weakly model dependent method for determining the $\rho R$ of the remaining Be ablator.

As shown in Fig. 1b, a much larger fraction of the produced KO-P's exit the 105 mg/cm$^2$ ablator than the 210 mg/cm$^2$ ablator; ~$8\times10^{10}$ KO-P's exit the 105 mg/cm$^2$ ablator, while only ~$3\times10^{9}$ KO-P's exit the 210 mg/cm$^2$ ablator, which corresponds to a KO-P to neutron yield ratio ($Y_{KO\text{-}P}/Y_n$) of ~$1.5\times10^{-5}$ and ~$5.7\times10^{-7}$, respectively. These KO-P protons are born in the ~30 μm and ~10 μm outermost region of the fuel for the 105 mg/cm$^2$ and 210 mg/cm$^2$ ablator case, respectively. The exact trend of how the $Y_{KO\text{-}P}/Y_n$ ratio varies with increasing $\rho R$ of the Be ablator is illustrated by the filled circles in Fig. 2. In addition, it should be noted that the build up of $^3$He in the fuel causes D$^3$He reactions to occur. These reactions produce 14.7-MeV protons that in principle could affect the KO-P measurements. However, simulations indicate that the D$^3$He protons are fully ranged out as they are produced in the innermost 40-50 μm in the fuel (due to the strong temperature dependence of the D$^3$He fusion reaction). As a result, the D$^3$He-protons do not affect the KO-P measurements.

The CH ablator design, which contains naturally large amounts of H, can be diagnosed by measuring the absolute spectrum of KO-P's produced in the ablator. In particular, the shape of the measured KO-P spectrum provides information about the ablator $\rho R$. This is illustrated in Fig. 3, which shows simulations of two capsule implosions. The density and temperature profiles used for the fuel and ablator in these two simulations are shown in Fig. 3a. Once again, the density and temperature profiles for the fuel were kept the same, while the density profile for the ablator was changed artificially to illustrate the effect of a varying $\rho R$ on the shape of the KO-P spectrum. In the simulations, the ablator extends out to a radius of 150 μm (top figure) and 220 μm

(bottom figure) corresponding to an ablator $\rho R$ of 105 mg/cm$^2$ and 210 mg/cm$^2$, respectively. The resulting KO-P spectra, shown in Fig. 3b, indicate that the change of the ablator $\rho R$ has a significant impact on the shape of the KO-P spectrum. In contrast, the shape of the KO-P spectrum is not affected significantly by ablator-density-profile variations, even though the spatial birth profile of the KO-P's depends strongly on the density profile. This is a consequence of the fact that the energy-slowing down of the KO-Ps is very weakly dependent on mass-density-profile variations. As shown in the references [6], the slowing down depends mainly on $\rho R$, while density and temperature effects play minor roles. Other effects, such as time evolution of the ablator $\rho R$ and fuel-shell mix play minor roles as well, as described in more detail in the next two paragraphs.

Time evolution of the ablator $\rho R$ has a small effect on the shape of the KO-P spectrum, which significantly simplifies the interpretation of the measured KO-P spectrum. This is illustrated by transporting KO-P's through density and temperature profiles simulated by the 1-D hydrocode LILAC [27] at different times for a hydroequivalent capsule implosion at OMEGA. The density and temperature profiles used are illustrated in Figs. 4a and 4b, which show the density and temperature profiles at bang time (BT), BT-100 ps, and BT+80 ps for an imploding DT-gas filled CH capsule at OMEGA (a total burn duration of ~180 ps was simulated for this particular implosion). The resulting KO-P spectra for the different times are shown in Fig. 4c. Each simulated KO-P spectrum was determined assuming a steady-state condition for 60 ps. Despite the fact that KO-P's are produced before and after bang time, the KO-P spectrum produced at bang time dominates and well represents the burn-weighted spectrum; an indication that a time-integrated measurement of the KO-P spectrum will provide accurate information about the ablator $\rho R$ at bang time. In addition, using a hydroequivalent OMEGA implosion to study how the time-evolution of the ablator $\rho R$ affects the KO-P spectrum is valid as the burn duration and percentage variation of the ablator $\rho R$ during burn are similar as for an ignition-scaled NIF-capsule implosion.

Fuel-ablator mix plays a minor role as well. As the fuel density and temperature is much lower in the mixed region than in the clean region, the radial source profile of the primary neutrons is not affected by mix to a level that the KO-P spectrum is significantly

altered. However, the fuel-ablator mix does alter the ablator-density-profile, but this has no impact on the shape of the KO-P spectrum as already discussed.

Although $Y_{KO\text{-}P}$ is subject to significant spatial-yield variations caused by magnetic fields surrounding an implosion, an average $Y_{KO\text{-}P}$ determined from several measurements can be used to infer a spatially averaged $\rho R$ of the CH ablator as discussed in reference [12]. By using a relatively simple model of an implosion, the $Y_{KO\text{-}P}$, normalized to the neutron yield $Y_n$, can be related to the ablator $\rho R$ by

$$\frac{Y_{KO-P}}{Y_n} = \frac{\gamma \sigma_p}{(\gamma + 12) m_p} \xi(\rho R) \rho R , \qquad (1)$$

where $\gamma = n_H/n_C$ ($\gamma \approx 1.4$ for CH); $\sigma_p$ is the total cross section for the np-elastic scattering process; $m_p$ is the proton mass; and $\xi(\rho R)$ is a function describing the fraction of escaping KO-P's. Typically ~200 mg/cm$^2$ of the ablator $\rho R$ remain at bang time for an ignition-capsule implosion, which would generate a KO-P yield of $\sim 10^{-3} \cdot Y_n$. As $Y_{KO\text{-}P}$ is directly proportional to $\rho R \cdot Y_n$, and the ablator $\rho R$ and $Y_n$ are strongly dependent on the laser drive (a 30-40% variation in the laser drive changes the ablator $\rho R$ by a factor of ~2 and the $Y_n$ by a factor of 10 or more), measurements of $Y_{KO\text{-}P}$ should allow studies of the ablator $\rho R$ and the drive-physics. To understand quantitatively how the $Y_{KO\text{-}P}/Y_n$ ratio varies with the $\rho R$ of the remaining CH ablator, several simulations of a capsule implosion were performed. In the simulations, the same density and temperature profiles of the fuel were used as for the capsule implosions shown in Fig. 3a, while the profile of the CH ablator was artificially changed. The resulting data from these simulations, which are shown in Fig. 5, indicate that the $Y_{KO\text{-}P}/Y_n$ ratio saturates at $\sim 10^{-3}$ for $\rho R$s above 150 mg/cm$^2$. In addition, the escaping fraction reduces from 50% to 10% (relative to the number of produced KO-P's) as the $\rho R$ increases from practically zero to ~250 mg/cm$^2$. Very relevant to this discussion is that these measurements are not affected significantly by the KO-P's produced in the fuel (due to the ~1% residual H) as the yield of the escaping KO-P's, produced in the fuel, is typically orders of magnitude lower than the yield of the escaping KO-P's produced in the CH ablator (see Figs. 2 and 5 for a qualitative comparison). Even at very low ablator $\rho R$s, the number of escaping KO-P's coming from

the CH ablator dominates the number of escaping KO-P's coming from the fuel. As a result, the measured $Y_{KO\text{-}P}/Y_n$ ratio can be used to diagnose the CH ablator for $\rho R$s up to ~200 mg/cm$^2$.

## III. Diagnosing the ablator $\rho R$ of capsule implosions filled with Hydrogen-Deuterium-Tritium (HDT) fuel

Prior to the first ignition experiments, capsules with a Cu-doped Be ablator (or Ge-doped CH ablator), more Deuterium-lean fuel mixtures and H-dopant levels up to 25% (by atom) in the fuel will be imploded to primarily reduce the primary neutron yield. To keep these implosions hydrodynamically equivalent to an ignition-capsule implosion, and to maintain the cryogenic Tritium fuel layering capabilities, stringent requirements on the fuel composition are applied. Two examples of Deuterium-lean fuel compositions that are being considered are: 22% H: 8% D: 70% T and 25% H: 0.5% D: 75% T. With a significantly higher H content in the fuel than in the ignition-capsule implosion, the HDT-filled Be capsule implosions are more suitable to diagnose using KO-P's as $Y_{KO\text{-}P}$ increases and $Y_n$ decreases resulting in a significantly higher signal-to-background (*S/B*) ratio [28]. This is also illustrated in Fig. 6, which shows simulated KO-P spectra (normalized by $Y_n$) for the 22%-H-filled-, 25%-H-filled-Be capsule implosions and the failed ignition-capsule implosion. Even though the simulated $Y_n$ for the 22%- and 25%-H-filled Be capsule implosion is ~4.5 and ~66 lower, respectively, than for the failed ignition-capsule implosion, the KO-P yield is in fact ~5 times higher and only ~2.5 times lower, respectively. As a result, the *S/B* ratio is 22 and 25 times higher, respectively, than the *S/B* ratio for the failed ignition-capsule implosion. A detailed discussion of the absolute *S/B* ratios can be found in the next section. In addition, as the Be-ablator profile is identical for these capsule implosions, the same high-energy endpoint of 10 MeV was simulated.

## IV. Proposed ablator $\rho R$ measurements at the NIF

The plan is to field several compact CR-39 based proton spectrometers (the spectrometer housing is less than 5 cm in diameter) [6] at various locations around an implosion to diagnose $\rho R$ and $\rho R$ modulations of the remaining ablator at bang time. As

the CR-39 efficiency for detecting KO-P's and background neutrons is 100% and about $6\times10^{-5}$ [29], respectively, the dynamic range of the spectrometer is determined mainly by the allowed range of spectrometer distances to the implosion, signal statistics and signal saturation. About ~$10^3$ signal counts are required for inferring an ablator $\rho R$ from either the high-energy end point or the shape of the KO-P spectrum, and ~$10^5$ signal counts per $cm^2$ are required for the CR-39 to saturate [6]. With an active spectrometer area of ~1 $cm^2$, a range of allowed spectrometer distances of 40 to 550 cm to the implosion and $1/R^2$-scaling of the detected KO-P signal, absolute spectra can be measured accurately for KO-P yields ranging from ~$1\times10^7$ to ~$4\times10^{11}$. This absolute yield range combined with the simulated results shown in Figs. 2 and 5, which illustrate the $Y_{KO\text{-}P}/Y_n$ ratio as a function of the ablator $\rho R$, are used to establish the absolute KO-P yield as a function of $Y_n$ and $\rho R$ for the different ablators (see Fig 7). The Be-ablator curves, shown in Fig. 7a, indicate a tolerable $Y_n$ range of ~$5\times10^9$ to >$10^{18}$ [the solid and dashed line is for the failed ignition-capsule implosion (with ~1%-residual H) and 25%-H-filled-Be capsule implosion, respectively]. However, as the $\rho R$ of the Be ablator approaches 240 $mg/cm^2$, $Y_{KO\text{-}P}$ decreases significantly to the point where the *S/B* ratio is well below one. At this point, the CR-39 saturation is dictated mainly by the neutron background. Based on the information in ref. [29], an upper $Y_n$ limit of ~$5\times10^{16}$ is determined for a spectrometer positioned at 550 cm to the implosion. In contrast, the tolerable $Y_n$ range for the CH-ablator case is dictated only by the measurable $Y_{KO\text{-}P}$ range, resulting in a range of ~$10^{10}$ to ~$3\times10^{16}$ as shown in Fig. 7b.

Maximizing the *S/B* ratio is essential to the proposed KO-P measurements. Using a standard-counting technique (SCT) [6], utilized for more than a decade, a *S/B* range of ~0.01 - 10 and ~0.2 - 200 is obtained for the failed ignition-capsule implosion and 25%-H-filled-Be capsule implosion, respectively (see Fig. 8a). In the case of the CH ablator, the *S/B* varies from ~1 to ~100 as illustrated in Fig. 8b. In both cases, the *S/B* is independent of $Y_n$ and only varies with varying ablator $\rho R$. By applying the coincidence-counting technique (CCT) [30-31] to the low *S/B* cases ($S/B \leq 1$), the *S/B* ratios are improved significantly as shown in both Figs. 8a and 8b for $Y_n < 10^{16}$ [32]. For increasing neutron yields above $10^{16}$ the CCT gets less effective as the background increases; a result of an increasing number of random coincidences of neutron-induced tracks on the

front and back side of the CR-39. Both in terms of signal and *S/B*, it is clear that the KO-P measurement technique will be very useful for determining $\rho R$ and $\rho R$ modulations of the remaining ablator for a large range capsule implosions at the NIF.

## V. Measurements performed at OMEGA

Diagnosing shell $\rho R$ and $\rho R$ modulations of gas-filled CH-capsule implosions have been performed routinely at OMEGA for more than a decade [33-35]. In many of those experiments, which are similar to the ablator measurements proposed at the NIF, up to nine charged-particle spectrometers were fielded around an implosion. An example of resulting data from those experiments is illustrated in Fig. 9, which shows a subset of four KO-P spectra obtained from a single high-adiabat implosion involving a capsule with a 27 μm CH shell filled with 3 atm of DT gas (shot 39894). $\rho R$'s varying from 20 to 50 mg/cm$^2$ were inferred from the Monte-Carlo simulated fits (red spectra) to the measured spectra. Very relevant to this work is that Li *et al.* demonstrated in ref. [33] that these low-mode $\rho R$ modulations, which are often observed in the charged-particle data obtained at OMEGA, are strongly connected to the laser-power imbalance.

A complementary approach for quickly assessing the $\rho R$ value in a certain direction is to look at what energy the KO-P spectrum flattens out; in the case of the 20 mg/cm$^2$ and 50 mg/cm$^2$, the spectrum flattens out at ~12.5 MeV and ~10 MeV, respectively. The reason for this correlation can be addressed by using a simple ice-block-implosion model to simulate KO-P spectra for different $\rho R$s of the CH shell. Fig. 10a shows the ice-block-implosion model used in which the shell density was kept constant, while the shell thickness was increased in steps of 10 μm (a constant electron temperature of 500 eV was used as well). For simplicity a neutron point source at the center of the implosion was also used in these simulations. The resulting KO-P spectra, shown in Fig. 10b, illustrate a strong correlation between the location of the "knee" in the KO-P spectrum and $\rho R$. The reason for this correlation is that the maximum energy of the escaping KO-P's produced at 60, 50, 40 and 30 μm can not be higher than 14, 12.5, 10.2 and 9.3 MeV, respectively, which results in a KO-P spectrum that displays a high-energy edge with a slope that extends down in energy depending on the $\rho R$.

## VI. Summary

We propose to accurately determine the areal density ($\rho R$) of the remaining ablator at bang time for several types of NIF-capsule implosions using charged-particle spectrometry. By fielding several very compact charged-particle spectrometers in different positions around the implosion, $\rho R$ and $\rho R$ modulations of the remaining ablator can be obtained through absolute measurements of yield and spectra of knock-on protons (KO-P). The results from several simulations of ignition-capsule and H-filled capsule implosions at the NIF and experiments performed at OMEGA clearly indicate that measurements of KO-P spectrum at various locations around an implosion can provide accurate information about $\rho R$ and $\rho R$ modulations of the remaining ablator for a large range of capsule implosions at the NIF.

## References


1. G.H. Miller, E.I. Moses and C.R. Wuest, Nucl. Fusion **44**, S228 (2004).
2. J.D. Lindl, P. Amendt, R.L. Berger, S.G. Glendinning, S.H. Glenzer, S.W. Haan, R.L. Kauffman, O.L. Landen, and L.J. Suter, Phys. Plasmas **11**, 339 (2004).
3. S.W. Haan, M.C. Hermann, T.R. Dittrich, A.J. Fetterman, M.M. Marinak, D.H. Munro, S.M. Pollaine, J.D. Salmonson, G.L. Strobel, and L.J. Suter, Phys. Plasmas **12**, 056316 (2005).
4. S.W. Haan, P.A. Amendt, T.R. Dittrich, B.A. Hammel, S.P. Hatchett, M.C. Herrmann, O.A. Hurricane, O.S. Jones, J.D. Lindl, M.M. Marinak, D. Munro, S.M. Pollaine, J.D. Salmonson, G.L. Strobel and L.J. Suter, Nucl. Fusion **44,** S171 (2004).
5. D.H. Munro, P.M. Celliers, G.W. Collins, D.M. Gold, L.B. Da Silva, S.W. Haan, R.C. Cauble, B.A. Hammel, and W.W. Hsing, Phys. Plasmas **8**, 2245 (2001).
6. F. H. Séguin, J. A. Frenje, C. K. Li, D.G. Hicks, S. Kurebayashi, J.R. Rygg, B.-E. Schwartz, and R.D. Petrasso, S. Roberts, J.M. Soures, D.D. Meyerhofer, T.C. Sangster, J.P. Knauer, C. Sorce, V.Yu. Glebov, C. Stoeckl, T.W. Phillips , R. J. Leeper, K. Fletcher and S. Padalino Rev. Sci. Instrum. **74**, 975 (2003).
7. S.P. Hatchett explored the idea of using knock-on deuterons (KO-D) to diagnose the Beryllium ablator. However, it turned out that this was not feasible as the KO-D's have a relatively short range.

8. S. Kurebayashi, J.A. Frenje, F.H. Seguin, J.R. Rygg, C.K. Li, R.D. Petrasso, V.Yu. Glebov, J.A. Delettrez, T.C. Sangster, D.D. Meyerhofer, C. Stoeckl, J.M. Soures, P.A. Amendt, S.P. Hatchett, and R.E. Turner Phys. Plasmas **12**, 032703 (2005).
9. C. K. Li and R. D. Petrasso, Phys. Rev. Lett. **70**, 3059 (1993).
10. H. Nakaishi, N. Miyanaga, H. Azechi, M. Yamanaka, T. Yamanaka, M. Takagi, T. Jitsuno, and S. Nakai, Appl. Phys. Lett. **54**, 1308 (1989).
11. C.K. Li, F. H. Séguin, D. G. Hicks, J.A. Frenje, K.M. Green, S. Kurebayashi, R.D. Petrasso, D.D. Meyerhofer, J.M. Soures, V.Yu. Glebov, R.L. Keck, P.B. Radha, S. Roberts, W. Seka, S. Skupsky, C. Stoeckl, and T.C. Sangster Phys. Plasmas **8**, 4902 (2001).
12. J. A. Frenje, C.K. Li, F.H. Séguin, S. Kurebayashi, R.D. Petrasso, J.M. Soures, J. Delettrez, V.Yu. Glebov, D.D. Meyerhofer, P.B. Radha, S. Roberts, T.C. Sangster, S. Skupsky, and C. Stoeckl Phys. Plasmas **9**, 4719 (2002).
13. F.H. Séguin C.K. Li, J.A. Frenje, S. Kurebayashi, R.D. Petrasso, F.J. Marshall, D.D. Meyerhofer, J.M. Soures, T.C. Sangster, C. Stoeckl, J.A. Delettrez, P.B. Radha, V.A. Smalyuk, and S. Roberts, Phys. Plasmas **9**, 3558 (2002).
14. D.G. Hicks, C.K. Li, F.H. Séguin, A.K. Ram, J.A. Frenje, R.D. Petrasso, J.M. Soures, V.Yu. Glebov, D.D. Meyerhofer, S. Roberts, C. Sorce, and C. Stöckl T.C. Sangster and T.W. Phillips, Phys. Plasmas **7**, 5106 (2000).
15. D.C. Wilson, R.L. Singleton Jr., J.P. Grondalski, N.M. Hoffman, A. Nobile, Jr., F.H. Séguin, J.A. Frenje, C.K. Li, and R.D. Petrasso, Rev. Sci. Instrum. **77**, 10E711 (2006).
16. D.G. Hicks, B. Spears, C. Sorce, P. Celliers, O. Landen, G. Collins, T. Boehly, Bull. of Am. Phys. Soc. **52**, (2007).
17. R.E. Olson, G.A. Rochau and R.J. Leeper, Bull. of Am. Phys. Soc. **52**, (2007).
18. R.E. Olson, R.J. Leeper, A. Nobile, J.A. Oertel, G.A. Chandler, K. Cochrane, S.C. Dropinski, S. Evans, S.W. Haan, J.L. Kaae, J.P. Knauer, K. Lash, L.P. Mix, A. Nikroo, G.A. Rochau, G. Rivera, C. Russell, D. Schroen, R. J. Sebring, D. L. Tanner, R. E. Turner, and R. J. Wallace, Phys. Plasmas **11**, 2778 (2004).
19. C.K. Li, D.G. Hicks, F.H. Séguin, J.A. Frenje, R.D. Petrasso, J.M. Soures, P.B. Radha, V.Yu. Glebov, C. Stoeckl, D.R. Harding, J.P. Knauer, R. Kremens, F.J.

Marshall, D.D. Meyerhofer, S. Skupsky, S. Roberts, C. Sorce T.C. Sangster, T.W. Phillips, and M. D. Cable, Phys. Plasmas **7**, 2578 (2000).

20. S.W. Haan, P.A. Amendt, D.A. Callahan, T.R. Dittrich, M.J. Edwards, B.A. Hammel, D.D. Ho, O.S. Jones, J.D. Lindl, M.M. Marinak, D.H. Munro, S.M. Pollaine, J.D. Salmonson, B.K. Spears, and L.J. Suter, Fusion Sci. Technol. **51**, 509 (2007).
21. S.W. Haan, P.A. Amendt, D.A. Callahan, M.C. Herrmann, P.A. Amendt, D.A. Callahan, T.R. Dittrich, M.J. Edwards, O.S. Jones, M.M. Marinak, D.H. Munro, S. M. Pollaine, J.D. Salmonson, B.K. Spears, and L.J. Suter, Fusion Sci. Technol. **49**, 553 (2006).
22. A. Nikroo, K.C. Chen, M.L. Hoppe, H. Huang, J.R. Wall, H. Xu, M.W. McElfresh, C.S. Alford, R.C. Cook, J.C. Cooley, R. Fields, R. Hackenberg, R.P. Doerner and M. Baldwin, Phys. Plasmas **13**, 056302 (2006).
23. J. Biener, P. B. Mirkarimi, J.W. Tringe, S.L. Baker, Y.Wang, S.O. Kucheyev, N.E. Teslich, K.J.J. Wu, A.V. Hamza, C. Wild, E. Woerner, P. Koidl, K. Bruehne, and H.-J. Fecht, Fusion Sci. Technol. **49**, 737 (2006).
24. The diamond-ablator design can in principle be diagnosed using the same method to that of Be.
25. R.D. Petrasso, C.K. Li, M.D Cable, S.M. Pollaine, S.W. Haan, T.P. Bernat, J.D. Kilkenny, S. Cremer, J.P. Knauer, C.P. Verdon, and R.L. Kremens, Phys. Rev. Letters **77**, 2718 (1996).
26. The effect of fuel-ablator mix results in a $\rho R$ value that reflects the clean ablator.
27. J. Delettrez, Can. J. Phys. **64**, 932 (1986).
28. As CR-39 detectors are used in the proton spectrometers, the signal ($S$) scales with hydrogen content in the fuel times primary neutron yield ($Y_n$) [19], while the background ($B$), which is mainly due to neutrons, only scales with $Y_n$ [29]. As a result, the $S/B$ ratio increases with increasing hydrogen content in the fuel.
29. J.A. Frenje, C.K. Li, F.H. Séguin, D.G. Hicks, S. Kurebayashi, R.D. Petrasso, S. Roberts, V.Yu. Glebov, D.D. Meyerhofer, T.C. Sangster, J.M. Soures, C. Stoeckl, C. Chiritescu, G.J. Schmid, and R.A. Lerche, Rev. Sci. Instrum. **73**, 2597 (2002).
30. D.T Casey, J.A. Frenje, S.C. McDuffee, C.K. Li, J.R. Rygg, F.H. Séguin, R.D. Petrasso, V.Yu. Glebov, D.D. Meyerhofer, S. Roberts, and T.C. Sangster, "The CR-

39 Coincidence Counting Technique for Enhanced Signal-to-Background in a Large Range of Charged-Particle and Neutron Measurements at OMEGA and the NIF", Bull. of Am. Phys. Soc. 52, 208 (2007).

31. D.T Casey, J. A. Frenje, C. K. Li, J.R. Rygg, C.K. Li, S.C. McDuffee, M. Manuel R.D. Petrasso, V.Yu. Glebov, T.C. Sangster, D.D. Meyerhofer, S. Roberts P. Song, and M. Moran, "Minimizing background at the Magnetic Recoil Spectrometer (MRS) at OMEGA and the National Ignition Facility (NIF)", to be submitted to Rev. Sci. Instrum (2008).
32. The CCT utilizes the fact that a signal event produces a track on both the front and back side of a thin piece of CR-39, while a neutron-background event produces only a track on either the front or back side of the CR-39. By correlating the front and back side scans of the CR-39 data, most of the background is rejected, which significantly improves the *S/B*.
33. C.K. Li, F.H. Séguin, J.A. Frenje, R.D. Petrasso, R. Rygg, S. Kurebayashi, B. Schwartz, R.L. Keck, J.A. Delettrez, J.M. Soures, P.W. McKenty, V.N. Goncharov, J.P. Knauer, F.J. Marshall, D.D. Meyerhofer, P.B. Radha, S.P. Regan, T.C. Sangster, W. Seka, and C. Stoeckl, Phys. Plasmas **10**, 1919 (2003).
34. J.A. Frenje, C.K. Li, F.H. Séguin, J. Deciantis, S. Kurebayashi, J.R. Rygg, R.D. Petrasso, J. Delettrez, V.Yu. Glebov, C. Stoeckl, F.J. Marshall, D.D. Meyerhofer, T.C. Sangster, V.A. Smalyuk, and J.M. Soures, Phys. Plasmas **11**, 2798 (2004).
35. C. K. Li, F. H. Séguin, J. A. Frenje, R.D. Petrasso, J.A. Delettrez, P.W. McKenty, T.C. Sangster, R.L. Keck, J.M. Soures, F.J. Marshall, D.D. Meyerhofer, V.N. Goncharov, J.P. Knauer, P.B. Radha, S.P. Regan, and W. Seka, Phys. Rev. Lett. **92**, 205001 (2004).

Figure 1: Simulations of two Be-capsule implosions that fail to ignite. (a) Same density and temperature profiles were used for the fuel, while different density profiles were used for the Be ablator, i.e., the ablator extended out to a radius of 150 μm (top figure) and 220 μm (bottom figure) corresponding to an ablator $\rho R$ of 105 mg/cm$^2$ and 210 mg/cm$^2$, respectively. DT fuel with ~1% of residual hydrogen (by atom) was used in the simulations. A primary neutron yield of $5.3\times10^{15}$ was computed for both implosions. (b) Simulated KO-P spectra for the two failed implosions. A high-energy endpoint at 10 MeV (top figure) and 6 MeV (bottom figure) was simulated for the implosion with an ablator $\rho R$ of 105 mg/cm$^2$ and 210 mg/cm$^2$, respectively. Only a small fraction of the produced protons exit the Be ablator; ~$8\times10^{10}$ KO-P's exit the 105 mg/cm$^2$ ablator, and ~$3\times10^{9}$ KO-P's exit the 210 mg/cm$^2$ ablator. These protons are born in the ~30 μm and ~10 μm outermost region of the fuel for the 105 mg/cm$^2$ and 210 mg/cm$^2$ ablator case, respectively. A yield reduction is notable at lower energies in the KO-P spectrum. This is caused by an increasing fraction of ranged out KO-P's as the birth energy of these protons decreases. The KO-P's are fully ranged out at a Be ablator $\rho R$ of ~260 mg/cm$^2$.

Figure 2: Simulated energy downshift (filled circles) and $Y_{KO\text{-}P}/Y_n$ ratio (open circles) as a function of $\rho R$ of the remaining Be ablator. The density and temperature profiles of the fuel were kept constant, while the ablator $\rho R$ was changed. As the abaltor $\rho R$ increases from zero to ~250 mg/cm$^2$, the $Y_{KO\text{-}P}$ decreases several orders of magnitude. The KO-P's are fully ranged out at an ablator $\rho R$ of ~260 mg/cm$^2$. A primary neutron yield of $5.3\times10^{15}$ was simulated for these implosions.

Figure 3: Simulations of two CH-capsule implosions that fail to ignite. (a) Same density and temperature profiles were used for the fuel, while different density profiles were used for the CH ablator, i.e., the ablator extended out to a radius of 150 μm (top figure) and 220 μm (bottom figure) corresponding to an ablator $\rho R$ of 105 mg/cm$^2$ and 210 mg/cm$^2$, respectively. Both implosions produced $5.3\times10^{15}$ primary neutrons. (b) Simulated KO-P spectra for the two failed implosions. As shown in (b), the shape of the KO-P spectrum can be used to diagnose the $\rho R$ of the CH ablator. An average $\rho R$ of the ablator can also

be inferred from the KO-P yield as described by Eq. (1). For the 105 mg/cm$^2$ and 210 mg/cm$^2$ case, a total KO-P yield of $4\times10^{12}$ (top figure) and $6\times10^{12}$ (bottom figure) was simulated, respectively.

Figure 4 (Color): (a) Simulated LILAC density profiles at three different times, i.e., at bang time (BT), BT-100 ps, and BT+80 ps for OMEGA shot 39894 (an imploding 3-atm DT filled 27 μm thick CH capsule, which is discussed in more detail in Section V). A total burn duration of ~180 ps (FWHM) was simulated for this particular shot when using a flux limiter of 0.06. (b) Corresponding simulated temperature profiles. (c) Simulated KO-P spectra for the three different times (each simulated spectrum was computed assuming a steady-state condition for 60 ps). Also shown in (c) is the total, burn-weighted KO-P spectrum, which is very similar in shape to the spectrum produced at bang time, indicating that the time evolution of the ablator $\rho R$ plays a minor role in the $\rho R$ analysis of the measured the KO-P spectrum.

Figure 5: Simulated $Y_{KO\text{-}P}/Y_n$ ratio (filled circles) and KO-P escaping fraction (open circles), $\xi$, as a function of $\rho R$ of the CH ablator. The density and temperature profiles of the fuel were kept constant (see Fig. 3a), while the density profile of the ablator was varied. As shown, the yield ratio saturates at ~150 mg/cm$^2$ and the escaping fraction $\xi$ decreases from ~50% to ~10% as the ablator $\rho R$ increases from zero to ~250 mg/cm$^2$.

Figure 6 (Color): Simulated KO-P spectra normalized by $Y_n$ for a Cu-doped Be ablator and DT fuel doped with 22% and 25% H (red and black lines). For comparison, the normalized KO-P spectrum for the failed ignition-capsule implosion is also shown (blue line). To maintain hydrodynamically equivalence to the ignition-capsule implosion, the fuel composition of the H-filled Be capsule implosions are: 22% H: 8% D: 70% T: and 25% H: 0.5% D: 75% T. The same density and temperature profiles were used in these simulations (see Fig. 1a top graph). A primary neutron yield of $1.2\times10^{15}$ and $7.9\times10^{13}$ were simulated for the 22%- and 25%-H-filled Be capsule implosion, respectively. Although these primary neutron yields are ~4.5 times and ~66 times lower than for the failed ignition-capsule implosion, $Y_{KO\text{-}P}$ is in fact ~5 times higher ($4.5\times10^{11}$) and only

~2.5 times lower ($3.3\times10^{10}$) for the 22%- and 25%-H-filled Be capsule implosion, respectively. As a result, the signal-to-background (*S/B*) ratios are improved significantly as discussed in Sections III and IV. The same high-energy endpoint of 10 MeV was simulated in all three cases, which involved a 105 mg/cm$^2$ Be ablator.

Figure 7: (a) Absolute $Y_{KO\text{-}P}$ as a function of $Y_n$ and $\rho R$ for the failed ignition-capsule implosion with ~1% residual H (solid lines) and 25%-H-filled-Be capsule implosion (dashed lines). (b) Absolute $Y_{KO\text{-}P}$ as a function of $Y_n$ and $\rho R$ for the CH-capsule implosion. In contrast to the Be-ablator data, $Y_{KO\text{-}P}$ increases with increasing $\rho R$. The grey areas in both graphs indicate the measurable $Y_{KO\text{-}P}$ and $Y_n$ ranges at the NIF. The upper $Y_n$ limit of $\sim5\times10^{16}$ is determined by detector saturation caused by the neutron background. In both figures, the lower and upper limits of the measurable $\rho R$s are also indicated.

Figure 8: (a) Signal-to-background (*S/B*) ratios as functions of $Y_n$ for the failed ignition-capsule implosion with ~1% residual H (solid lines) and 25%-H-filled Be capsule implosion (dashed lines). (b) *S/B* ratios as functions of $Y_n$ for the CH capsule implosion. The horizontal lines in both figures represent the *S/B* when a standard-counting technique (SCT) is applied to the data. As shown by the SCT curves, the *S/B* ratio is independent on $Y_n$; a result of the fact that the signal scales with $f(\rho R)\cdot Y_n$ and the background scales only with $Y_n$. A range of *S/B* ratios of ~0.01-10 and ~0.2-200 is obtained for the failed ignition-capsule implosion with ~1% residual H and 25%-H-filled Be capsule implosion, respectively, while a *S/B* ratio varying from ~1 to ~100 is obtained for CH capsule implosion. By applying the coincidence-counting technique (CCT) to the low *S/B* cases ($S/B \leq 1$), the *S/B* ratios are improved significantly for $Y_n < 10^{16}$. For increasing neutron yields above $10^{16}$, the CCT gets less effective due an increasing number of background induced random coincidences.

Figure 9 (Color): A subset of KO-P spectra measured simultaneously in four different directions for OMEGA implosion 39894 (3 atm of DT fuel in a 27 μm thick CH shell, illuminated by 60 laser beams delivering 23 kJ of laser energy in a 1-ns square pulse). Narrow-band-width spectrometers that only cover the high-energy portion of the spectrum were used in these measurements. Each spectrum has been normalized to the average KO-P yield of $1.5\times10^{8}$. With a measured neutron yield of $6.5\times10^{11}$, the average *S/B* ratio is ~10 when using the standard counting technique (SCT). The observed differences in the spectral shape are well modeled by the steady-state Monte-Carlo simulations (red spectra), which indicate significant low-mode $\rho R$ modulations, e.g., varying from 20 to 50 mg/cm$^2$. A quick assessment of the $\rho R$ value in a certain direction can be done by looking at what energy the KO-P spectrum flattens out; for the 20 mg/cm$^2$ and 50 mg/cm$^2$ the spectrum flattens out at ~12.5 MeV and ~10 MeV, respectively.

Figure 10 (Color): Modeling of high-adiabat implosions at OMEGA, using simple ice-block-implosion models, to illustrate the relationship between $\rho R$ and the shape of the KO-P spectrum. (a) The shell density of 20 g/cc was kept constant, while the shell thickness was increased in steps of 10 μm (a fixed $T_e$ of 500 eV was used as well). A neutron point source at the center of the implosion was also used in these simulations (b) Simulated KO-P spectra for four different $\rho R$s ranging from 20 to 80 mg/cm$^2$. The spectral shape, and in particular the location of the "knee" in the spectrum, depends strongly on $\rho R$. The reason for this is that the maximum energy of the escaping KO-P's produced at 60, 50, 40 and 30 μm can not be higher than 14, 12.5, 10.2 and 9.3 MeV, respectively. As a consequence, the high-energy edge displays a slope that extends down in energy depending on the $\rho R$.

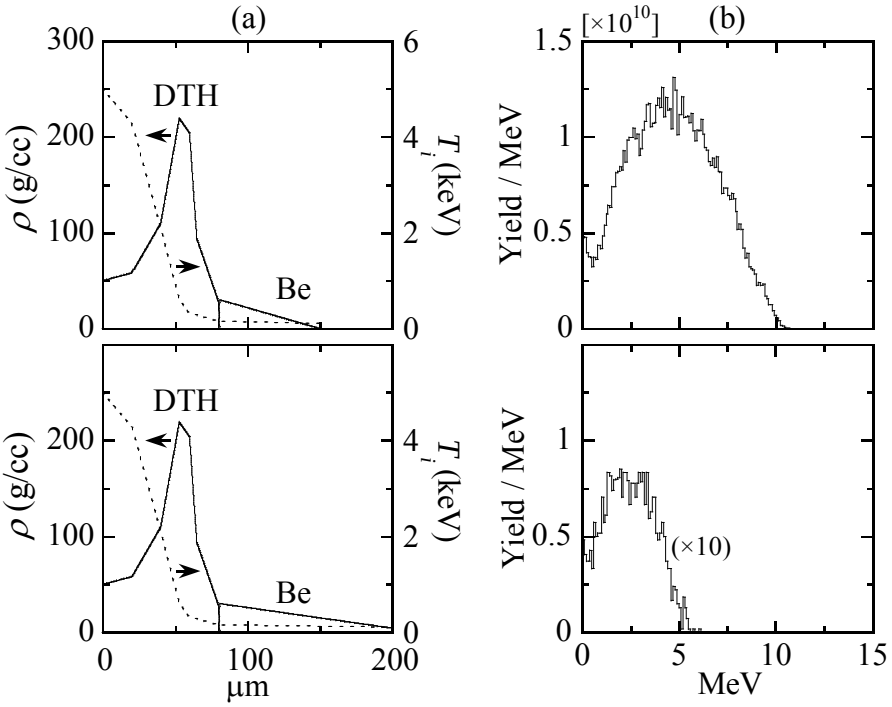


Fig. 1

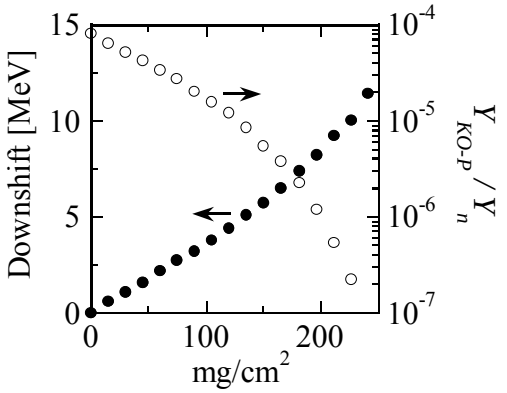


Fig. 2

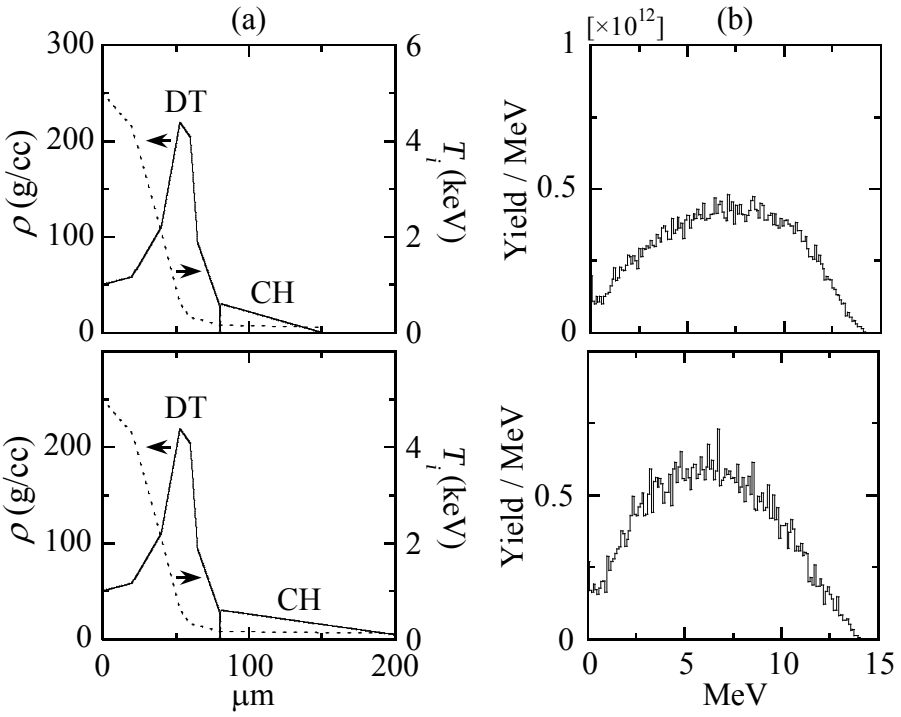


Fig. 3

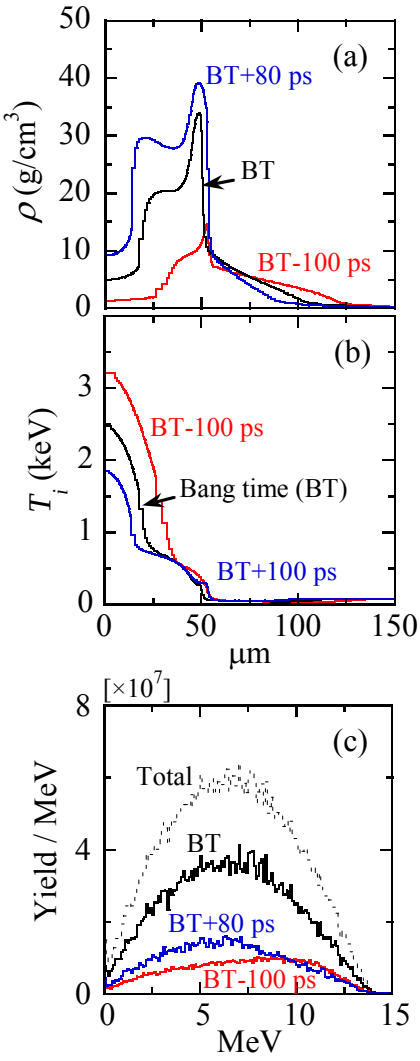
(a)
BT+80 ps
BT
BT-100 ps
ρ (g/cm3)
(b)
BT-100 ps
Bang time (BT)
BT+100 ps
Ti (keV)
μm
[×10^7]
(c)
Total
BT
BT+80 ps
BT-100 ps
Yield / MeV
MeV

Fig. 4

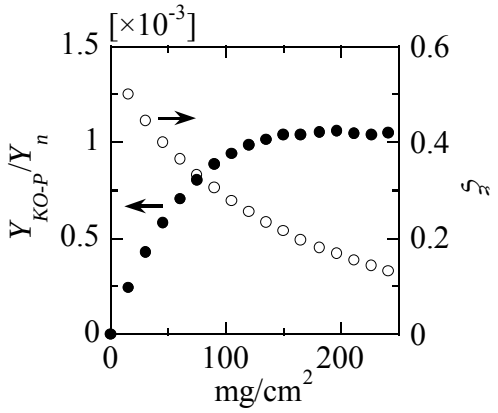


Fig. 5

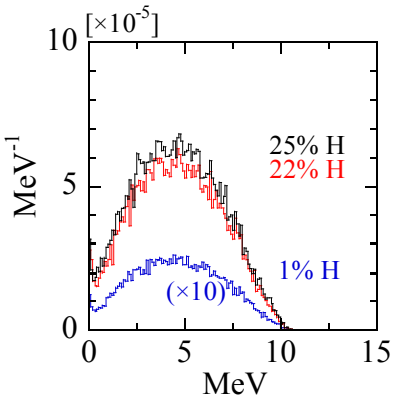


Fig. 6

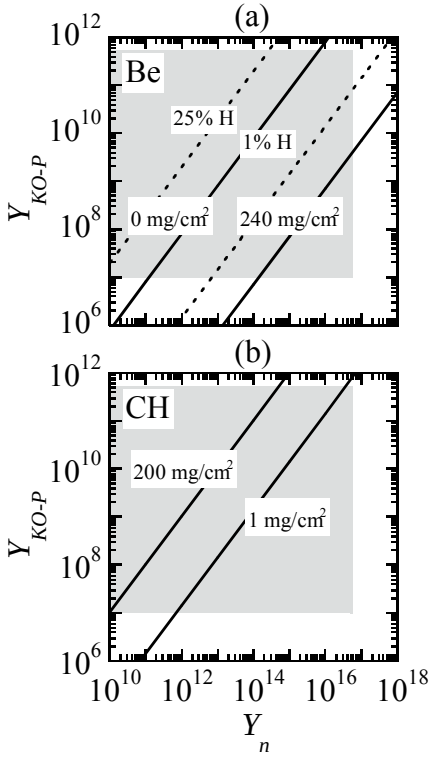
(a)
Be
25% H
1% H
0 mg/cm2
240 mg/cm2
(b)
CH
200 mg/cm2
1 mg/cm2
$Y_{KO-P}$
$Y_n$
$10^{6}$
$10^{8}$
$10^{10}$
$10^{12}$
$10^{14}$
$10^{16}$
$10^{18}$

Fig. 7

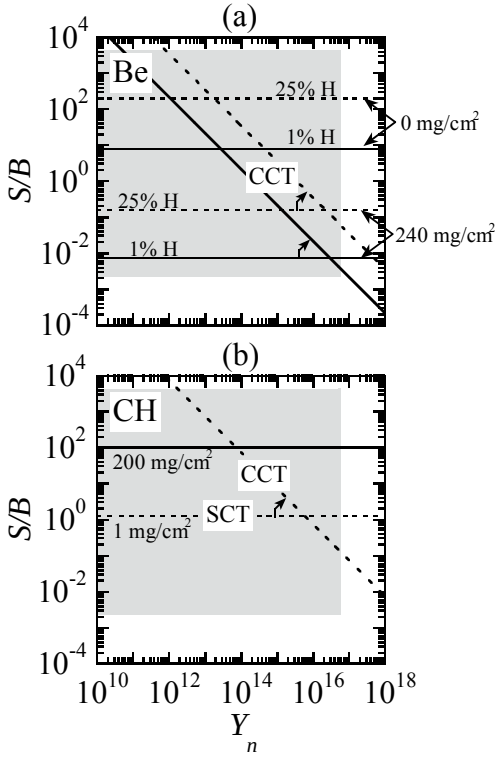
(a)
Be
25% H
1% H
CCT
25% H
1% H
0 mg/cm2
240 mg/cm2
(b)
CH
200 mg/cm2
CCT
SCT
1 mg/cm2
S/B
Yn

Fig. 8

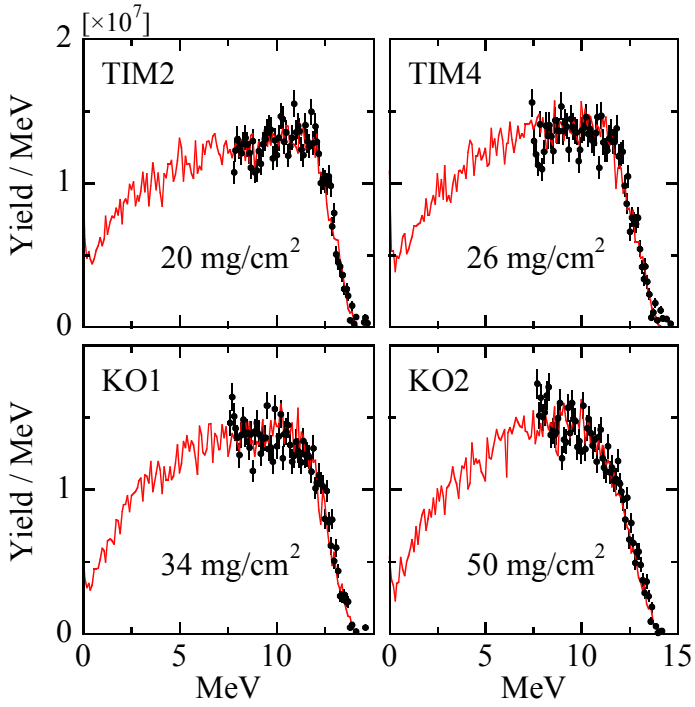
[×10^7]
2
1
0
Yield / MeV
TIM2
20 mg/cm^2
TIM4
26 mg/cm^2
KO1
34 mg/cm^2
KO2
50 mg/cm^2
0
5
10
15
MeV

Fig. 9

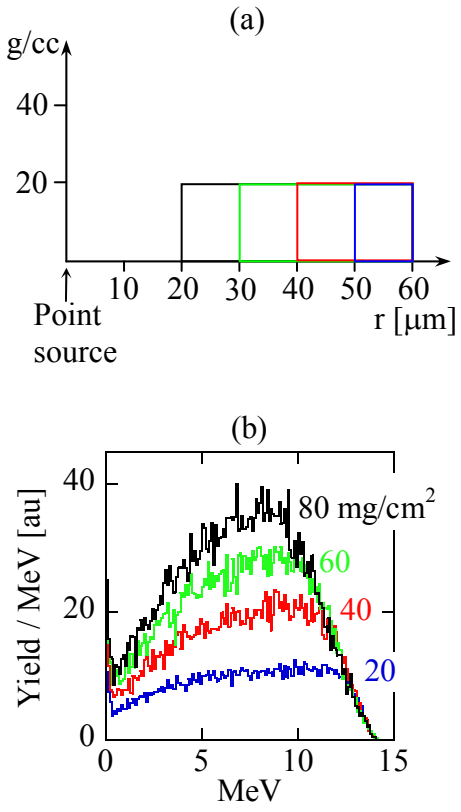
(a)
g/cc
40
20
10
20
30
40
50
60
Point
source
r [μm]
(b)
Yield / MeV [au]
40
20
0
0
5
10
15
MeV
80 mg/cm2
60
40
20

Fig. 10